2676–2681 *Nucleic Acids Research, 2010, Vol. 38, No. 8* *Published online 17 December 2009*
doi:10.1093/nar/gkp1069

Cell cycle-dependent variations in protein concentration

Natalie A. Cookson[1], Scott W. Cookson[1], Lev S. Tsimring[2] and Jeff Hasty[1,2,3,*]

[1]Department of Bioengineering, [2]BioCircuits Institute, [3]Molecular Biology Section, Division of Biology, University of California, San Diego, La Jolla, CA 92093, USA

Received August 19, 2009; Revised October 28, 2009; Accepted October 30, 2009

ABSTRACT

Computational modeling of biological systems has become an effective tool for analyzing cellular behavior and for elucidating key properties of the intricate networks that underlie experimental observations. While most modeling techniques rely heavily on the concentrations of intracellular molecules, little attention has been paid to tracking and simulating the significant volume fluctuations that occur over each cell division cycle. Here, we use fluorescence microscopy to acquire single cell volume trajectories for a large population of *Saccharomyces cerevisiae* cells. Using this data, we generate a comprehensive set of statistics that govern the growth and division of these cells over many generations, and we discover several interesting trends in their size, growth and protein production characteristics. We use these statistics to develop an accurate model of cell cycle volume dynamics, starting at cell birth. Finally, we demonstrate the importance of tracking volume fluctuations by combining cell division dynamics with a minimal gene expression model for a constitutively expressed fluorescent protein. The significant oscillations in the cellular concentration of a stable, highly expressed protein mimic the observed experimental trajectories and demonstrate the fundamental impact that the cell cycle has on cellular functions.

INTRODUCTION

Synthetic biology has emerged as an important field in the effort to quantitatively understand biological systems. (1,2). Bridging the gap between engineering and biology, this broad field includes a wide range of disciplines ranging from synthetic biochemistry to the recreation of life through artificial reconstruction of entire genomes (3,4). An important aspect of synthetic biology involves the design and construction of engineered gene circuits. Combining the powerful tools of molecular biology and computational modeling, synthetic gene networks can be designed to perform a specific biological function, and experimental data can be used to refine our quantitative understanding of the predicted behavior.

Our ability to synthesize and manipulate gene networks and study their behavior in living organisms has led to significant discoveries regarding some of the most fundamental cellular processes (5–8). In addition, the construction of synthetic networks according to the specifications of quantitative models has led to the refinement of our understanding of the principles of cellular regulation (9–12). Essential to this approach is the ability to develop computational models that can simulate and predict the behavior of cellular networks in growing and proliferating cells. In particular, the yeast *Saccharomyces cerevisiae* has served as an important eukaryotic model for cellular functions as fundamental as gene regulation and as complex as cell cycle orchestration (13–16). Models of gene regulation have been developed to elucidate sources of noise in gene expression and the effect of noise on fitness, to study the role of feedback in cellular networks, and have led to discoveries of novel network structure (6,17–29).

As we continue to develop these models as tools to refine our quantitative understanding of basic biological functions, an important and often overlooked contribution to network dynamics is the effect of volume fluctuations associated with the cell growth and division cycle. The majority of gene regulatory models rely on rate constants that are concentration dependent, yet typically the cellular volume is assumed to be constant. By ignoring volume fluctuations that affect concentrations in a quasi-periodic manner, the protein concentrations of 'constitutively expressed' genes are often considered to be constant, which can lead to incomplete conclusions regarding gene network behavior.

To address this issue, we measured volume dynamics along with gene expression in a population of yeast cells. We analyzed the growth characteristics of budding cells,

*To whom correspondence should be addressed. Tel: +1 858 534 2968; Email: hasty@bioeng.ucsd.edu

starting at birth, and generated a set of descriptive statistics governing the growth and division process. We used this information to develop an accurate cell division model, which takes into account the two distinct linear growth rates observed in the G1 and S phases. When combined with constitutive production of a fluorescent protein, the analysis reveals an oscillatory trend in the protein concentration over time. This effect of cellular growth and division is commonly overlooked, but it can play an important role in the behavior of both native and synthetic gene networks.

MATERIALS AND METHODS

Strain and cell culture

The yeast strain was created by targeted chromosomal integration of the pRS61-yv vector at the *gal1-10* locus of *S. cerevisiae* strain K699 (a, ADE2, ura3, his3, trp1, leu2). This vector was constructed using standard recombination techniques and contains the *gal1* promoter locus of *S. cerevisiae* driving production of the yeast-enhanced Venus fluorescent protein (yEVFP), a YFP variant (13). Cultures were grown in synthetic drop-out (SD) medium supplemented with all amino acids except uracil for selection of correct integration and containing 2% glucose. After selection, cultures were grown in SD supplemented with all amino acids and containing 2% galactose for full induction of the production of the yEVFP protein. Cultures were grown at 30°C for 12–18 h to an OD_{600} of 1.0 ± 0.25. In preparation for loading into the microfluidic device, the sample was passed back to an OD_{600} of 0.1 and allowed to grow for ~3 h to reenter exponential growth.

Data acquisition

Image acquisition was performed on a Nikon Diaphot TMD epifluorescent inverted microscope with a hardware-based autofocus controller (Prior Scientific, Rockland, MA, USA). Images were acquired using a Hamamatsu ORCA-ERG cooled charge-coupled device (CCD) camera, and fluorescence visualization was performed with narrow bandpass excitation and emission filters for YFP (Chroma, Inc., Rockingham, VT, USA). The cells were imaged inside a microfluidic chemostat as previously described (30).

Flow cytometry data acquisition

Flow cytometry data were acquired with a Becton-Dickinson FACSCalibur flow cytometer. The beads used for size calibration were obtained from Spherotech (SPHERO^{TM} Flow Cytometry Size Standard Kit). For each size bead, we collected 50 000 samples, and we used MATLAB (The MathWorks, Inc.) to calculate the mean forward scatter (FSC) measurement. We also took FSC and fluorescence data on the flow cytometer, using the K699 strain described above. To prepare the cells to be assayed, we grew them overnight in medium containing 2% galactose. In the morning, cells were passed to an OD_{600} of 0.05 and allowed to grow for 8 h. At this time, 1 ml of the culture was spun down at 8000 r.p.m. for 1 min, and the cells were resuspended in sterile phosphate buffered saline. The cells were run through the flow cytometer, and 50 000 cells were sampled. Again, MATLAB was used to analyze the flow cytometry data.

Computational model

MATLAB was used to model the growth and division of a population of yeast cells. The data from the trajectory analysis were used to generate histograms for each characteristic. These histograms were fit to Gaussian distributions, and the mean and standard deviation was calculated for each. These statistics were fed into the MATLAB model. Each cell was initialized using values drawn from a distribution based on this data. As cells were modeled from birth, the trends of the characteristics as a function of generation were also taken into account. That is, cells were initialized to a size drawn from the distribution of cells sizes at birth. Similarly, the fluorescence production rate, growth rate and growth phase characteristics were chosen from histograms of first generation measurements. After initialization, a cell was grown over time according to the current value of the growth rate, and fluorescence was produced based on the current value of fluorescence production.

The cell size was grown at the current value of the G1 growth rate until a threshold time was reached, set by the product of the cycle time and the fraction of time to be spent in G1. After this time, the cell size was grown at the current value of the S growth rate. The fluorescence was increased at a constant rate for the entire duration of the current cell cycle. When cell cycle end time was reached, the size and fluorescence of a cell was multiplied by the current value of ε, the fraction of volume to be retained by the mother at the time of division. For the next cycle, the values above were reset, again drawn from the distributions extracted from experimental data. The cells were grown for 836 min, the average length of the experimental trajectories. One thousand cells were simulated and compared with the experimental data, as described in the main text (see Supplementary Data for more details).

RESULTS AND DISCUSSION

In order to obtain a quantitative set of cell cycle growth characteristics, we tracked a large population of cells growing in a monolayer inside a microfluidic chemostat. The cells expressed a stable Venus YFP from the constitutive *gal1* promoter. A segmentation algorithm was applied to each image, providing an accurate area and position measurement for each cell at each time point (13,30). Volume for each cell was measured by calculating the major and minor axes for each cell area and fitting an ellipsoid to these values (Figure 1a–c). The height of the cell was assumed to be equal to the minor axis, unless the minor axis was larger than the height of the chamber. In that case, the height of the cell was set equal to the height of the chamber.

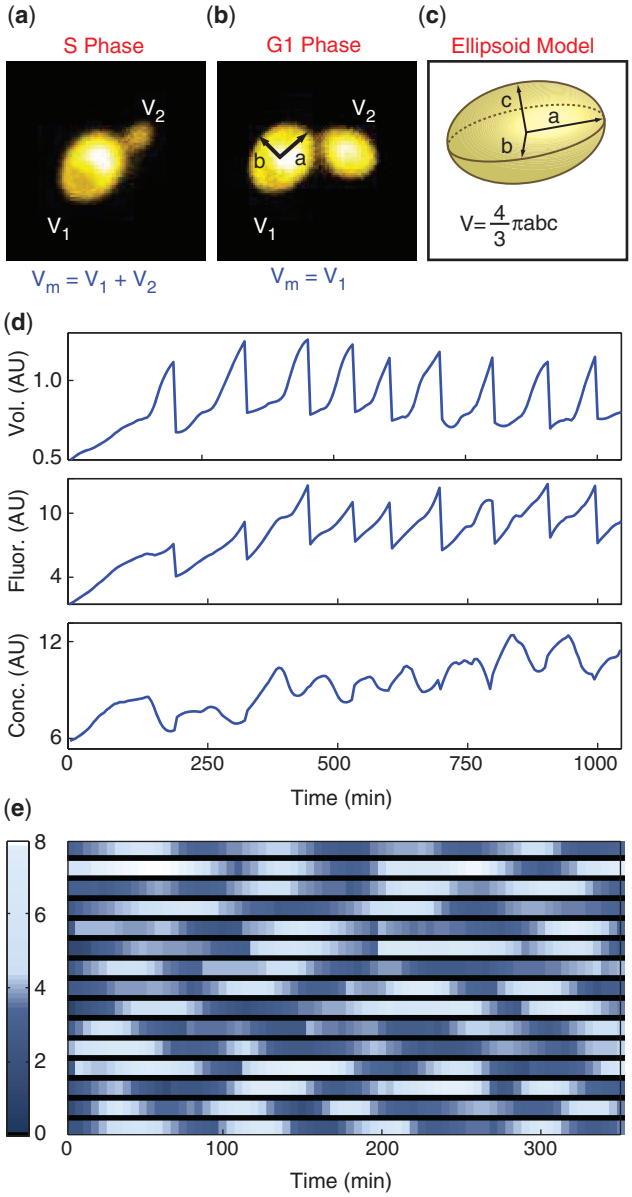

Figure 1. Single cell volume trajectories for a population of *S. cerevisiae*. (**a**) Assymetrically budding yeast cells were tracked through many generations of growth and division. During S phase, a mother cell begins to produce a small daughter cell. Until mitosis, the mother and daughter are connected, so their volumes are added together. (**b**) After mitosis, the mother and daughter cells have split, and their volumes are independent. During G1 phase, they grow very slowly as they prepare to produce their next buds. (**c**) Each cell was approximated to be an ellipsoid, with a major and minor axis (a and b, respectively). For larger cells with a minor axis greater than the height of the imaging chamber, the height of the cell was set equal to the height of the chamber; otherwise, the height of the cell was set equal to the minor axis. (**d**) Trajectories were generated for each cell, based on these volume measurements. The volume (top) clearly displays two different growth rates for G1 and S phase. Fluorescence (middle) was integrated over the entire area of each cell, and concentration (bottom) was calculated as total fluorescence divided by total volume. The combination of constant fluorescence production and bilinear volume growth yields oscillatory concentration trajectories. (**e**) Concentration trajectories for 15 cells show clear oscillations and a high degree of variability.

Cells were tracked from birth, and the volumes of a mother and bud cell were added together throughout each S phase (Figure 1a). The first appearance of the bud marks the beginning of S phase, so we used this visual cue to split each cell cycle into two growth phases. Using this time point for each cell cycle, we were able to measure the time spent in each phase and the growth rate of the cell in each phase (approximated by a linear fit to the slope of the volume). At the time of mitosis, the two volume trajectories were split and their volumes were considered separate starting at the beginning of the next G1 phase (Figure 1b). For the mother cell, this yields a discontinuity at the point of mitosis, with the volume dropping as the daughter receives a fraction of the volume and the mother retains the remaining fraction (Figure 1d, top).

YFP gene expression trajectories were generated by integrating the fluorescence signal over the entire cell at each time point (Figure 1d, middle), and concentration was calculated as the total fluorescence divided by the total volume (Figure 1d, bottom). The volume trajectories clearly show two distinct linear growth phases: a period of slow growth during the G1 phase of the cell cycle, and a period of faster growth as the cell begins to bud and progress through S phase towards mitosis. The production of YFP, on the other hand, remains roughly constant throughout each cell cycle. Because the tracking algorithm involves measuring the total fluorescence of a stable protein over each cell as a whole (including mother and bud, when appropriate), the production of YFP is calculated as the slope of the fluorescence trajectory between two budding events. The combination of these two phenomena leads to clear oscillations of the concentration trajectories. A density plot of 15 concentration trajectories demonstrates both the oscillations in individual trajectories as well as the large degree of cell-to-cell variability (Figure 1e).

For each cell, we tracked various growth characteristics to obtain distributions and determine trends in these characteristics (Figure 2a, Supplementary Data). Each cell included in the analysis was tracked from birth, in order to be able to confidently discern generation-dependent behaviors. That is, some statistics were observed to change over the first few generations of life, as the cell gradually reached a healthy adult size and growth rate. For example, the time required to complete each cell division cycle decreases over the first few generations (Figure 2b). This is a well known phenomenon, which has been observed using various techniques over the years (30,31).

Other traits that we observed and characterized include growth rates during both G1 and S phases, growth phase durations, fraction of volume loss at the end of each mitosis occurrence and cellular volume at the beginning and end of each cell cycle. While some characteristics are fairly constant, others vary greatly from cell to cell or even for an individual cell throughout its trajectory. Figure 2 shows all the characteristics that we quantified and how they vary by generation. For each characteristic, we quantified the mean and standard deviation across all

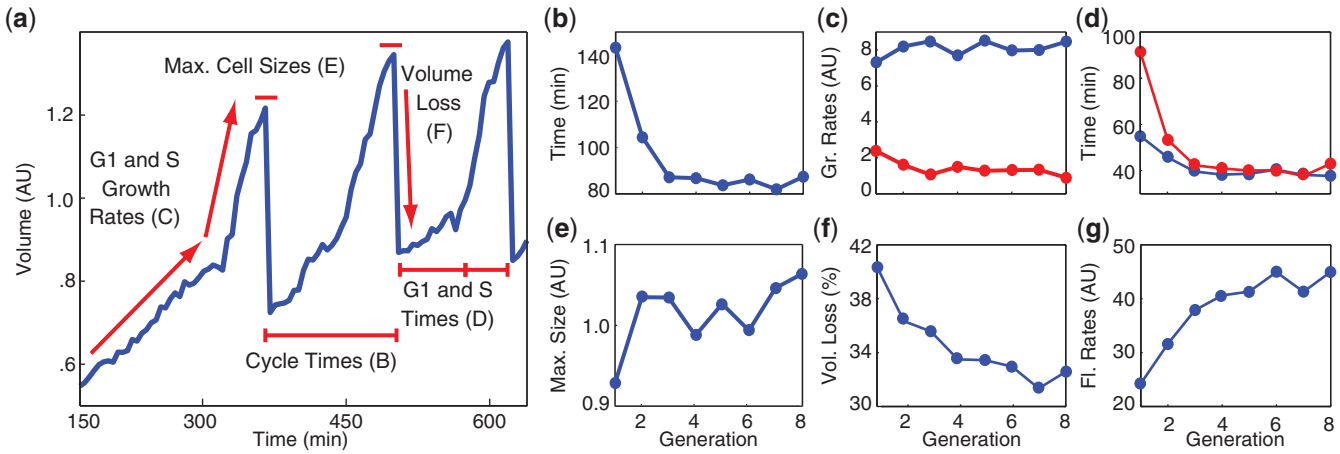

Figure 2. Volume growth and division statistics. (**a**) For each trajectory, we determined the mean and standard deviation of certain cell growth characteristics, starting at birth. These features were compared across each cell's various generations as well as across all trajectories. (**b**) The time to complete each cell cycle shows a downward trend over the first few generations. (**c**) The G1 (red) and S (blue) growth rates remain constant over time. (**d**) The time spent in each phase decreases over the first few generations, although the majority of time during the early generations is spent in G1. (**e**) The size of cells increases linearly with generation, although a larger jump in size of ~5% is observed between the first and second generations. (**f**) The percent of volume lost by a mother cell to its bud decreases on average for about five generations. (**g**) Finally, the fluorescence production rate is observed to increase over the first five or six generations, on average.

cells as well as across each individual cell's multiple generations.

Our volume trajectories demonstrate two clear growth phases, which could each be approximated by a linear growth rate. As expected, the G1 phase growth rate is significantly slower than the S phase growth rate (Figure 2c, S in blue, G1 in red). Interestingly, the growth rates in each phase remain constant throughout the generations observed. However, the time spent in each phase changes over the first three cycles, following a similar trend as the overall cell cycle time (Figure 2d). The time spent in G1 has a more extreme trend, with the time almost dropping in half over the first three generations. The S phase growth rate on the other hand speeds up a little as well, but our data demonstrate that the extra time required to complete the cell cycle early in life is spent mostly in the G1 phase. This is consistent with other studies that have demonstrated that changes in growth rate in different media conditions are mainly reflections of altered lengths of the G1 phase, with the duration of the S phase remaining fairly constant (32).

We also looked at cell size trends. For each cell, we examined how the maximum size reached at the end of each cell cycle varies over time, as well as how the mean of the maximum size compares to that of other cells (Figure 2e). As consistent with previous findings, our trajectories show a slight linear increase of cellular volume with age (33). However, by tracking cells from birth, we were also able to detect a more marked increase in size between the first and second generations of ~5% on average. We also tracked the percentage of volume lost by a mother to its new bud, which also had an interesting trend (Figure 2f). We found that it takes over five cycles for the value to level off to ~32%. This indicates that cells in their early generations bud daughter cells that are larger relative to their own size than they do throughout most of their lives.

These statistics and trends come together to form a comprehensive picture of how the volume changes in a quasi-periodic manner over many cellular generations, starting at birth. To determine how these volume fluctuations can affect the concentrations of intracellular proteins, we also measured fluorescence in the same cells. The fluorescence trajectories revealed a constant rate of protein production during each cell cycle (Figure 1d, middle). While fairly constant and linear, we found that the protein production rate for this constitutive promoter increases over the first five cycles before leveling off (Figure 2g). This could be due to many factors, such as a gradual building up of protein synthesis machinery, freeing up of resources originally dedicated to maturing into a healthy adult cell or a priority shift to metabolic gene expression as the cell matures.

We compiled all this information into a model that combines growth and division of budding yeast cells with constitutive YFP production. The model generates volume and fluorescence trajectories for newly budded cells for an arbitrary number of generations, which closely match the experimental results (Figure 3a and b). Histograms of volume, fluorescence and concentration distributions provide a good metric for comparing the experimental and simulated trajectories, and our simulations match the means and standard deviations of the experiments well (Figure 3c, d, and e).

Additionally, histograms from the microscopy data can be used as a standard for understanding flow cytometry data, which is commonly used to measure gene expression noise but is often difficult to interpret. The FSC measurement provided by a flow cytometer is believed to be proportional to the size of the object being measured, but it is unclear exactly what this value represents. In addition, the tendency of yeast cells to clump and their unusual shape due to asymmetric budding result in misleading size distributions. In order to compare our microscopy

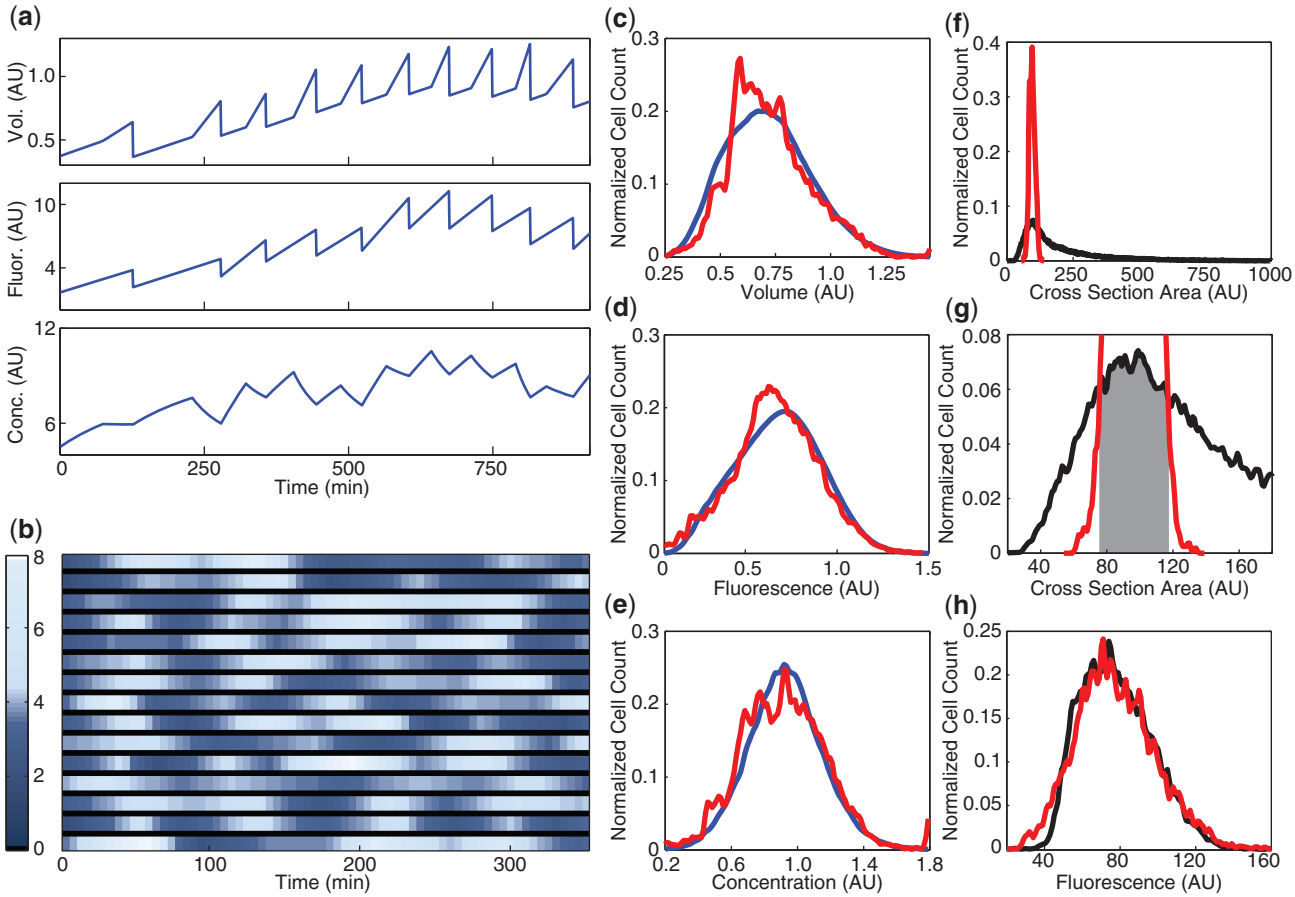

Figure 3. Comparison of experimental volume trajectories to model simulations and flow cytometry data. (**a**) Simulated volume (top), fluorescence (middle) and concentration (bottom) trajectories have similar trends as the experimental data (Figure 1). (**b**) Simulated concentration trajectories for 15 cells. (**c–e**) Comparisons of histograms of volume, fluorescence and concentration from the simulations (blue) and microscopy (red) data show well-matched means and standard deviations. (**f**) Comparison of size data from the flow cytometry (black) and microscopy (red) data demonstrates that the flow cytometer generates a deceptively wide distribution. (**g**) We can use the microscopy data to determine how to gate the flow cytometry data in order to sample just individual yeast cells. This metric yields a gate of 20% on either side of the FSC peak. (**h**) Using these gated cells, we can compare the fluorescence histograms from the flow cytometry and microscopy data, which yields very well-matched means and standard deviations.

size data to the FSC histogram provided by the flow cytometer, we had to first calibrate the FSC measurement to some physical characteristic of a yeast cell. To do this, we used spherical flow calibration beads of various diameters ranging from 2 to 15 μm. We ran these beads through the flow cytometer on the same settings we use to collect our yeast data, and we calculated the mean FSC measurement. In order to determine if the FSC was proportional to the length, area or volume of a sphere, we compared the diameter, diameter^2 and diameter^3 of the beads to the mean FSC value. It was clear from our data that the FSC measurement is proportional to the diameter of the bead (Supplementary Data).

Using the scope data as a reference for the true distribution of sizes for individual budding cells, we show that the FSC data provided by the flow cytometer yield a much wider distribution (Figure 3f), which translates to much higher fluorescence variability than is actually present in a healthy population of single cells. The presence of clumps of two or more cells as well as smaller particles (dead cells or media debris) creates a much wider size distribution than a homogeneous population of single cells would yield. We can use our microscopy size histogram to determine a metric for gating the flow cytometry size histogram about the mode of the distribution (Figure 3g). The fluorescence distribution of only the gated cells accurately reproduces the microscopy data (Figure 3h) and yields a coefficient of variation that is three times lower than that of the entire ungated data set.

As synthetic biology moves steadily toward the goal of developing accurate and predictive models of cellular behavior, it is clear that computational modeling will rely heavily on quantitative measurements of cellular phenomena. The cell division cycle is a highly dynamic and noisy process that affects a cell's behavior on many levels, and the fluctuations in cellular volume will affect the function of both native and synthetic gene networks. It will be important to account for these fluctuations in the construction of synthetic circuits designed to perform a specific function, such as to generate oscillations or toggle between two states, as they will inevitably network dynamics. In addition, determining the sources

and effects of noise in biological circuits is becoming increasingly critical, as we try to develop more detailed and robust models of genetic networks. These quasi-periodic fluctuations will have an impact on the study noise biology, which relies heavily on precise terms for the dilution of cellular components due to cell growth. Our results demonstrate the importance of accurately representing the complex growth trends of a population of cells in order to account for the effect that the resulting volume fluctuations have on the concentrations of intracellular components.

SUPPLEMENTARY DATA

Supplementary Data are available at NAR Online.

FUNDING

National Institute of General Medical Sciences of the National Institutes of Health (GM07933); Department of Energy Computational Science Graduate Fellowship (DE-FG02-97ER25308) to N.A.C.; Department of Defense National Defense Science and Engineering Graduate Fellowship to S.W.C. Funding for open access charge: National Institute of General Medical Sciences of the National Institutes of Health (GM07933).

Conflict of interest statement. None declared.

REFERENCES

1. Hasty,J., McMillen,D. and Collins,J.J. (2002) Engineered gene circuits. *Nature*, **420**, 224–230.
2. Sprinzak,D. and Elowitz,M.B. (2005) Reconstruction of genetic circuits. *Nature*, **438**, 443–448.
3. Iafolla,M. and McMillen,D. (2006) Extracting biochemical parameters for cellular modeling: a mean-field approach. *J. Phys. Chem. B*, **110**, 22019–22028.
4. Gibson,D.G., Benders,G.A., Andrews-Pfannkoch,C., Denisova,E.A., Baden-Tillson,H., Zaveri,J., Stockwell,T.B., Brownley,A., Thomas,D.W., Algire,M.A. *et al.* (2008) Complete chemical synthesis, assembly, and cloning of a mycoplasma genitalium genome. *Sci. STKE*, **319**, 1215.
5. Kepler,T.B. and Elston,T.C. (2001) Stochasticity in transcriptional regulation: origins, consequences, and mathematical representations. *Biophys. J.*, **81**, 3116–3136.
6. Ozbudak,E.M., Thattai,M., Kurtser,I., Grossman,A.D. and van Oudenaarden,A. (2002) Regulation of noise in the expression of a single gene. *Nat. Genet.*, **31**, 69–73.
7. Gardner,T.S., di Bernardo,D., Lorenz,D. and Collins,J.J. (2003) Inferring genetic networks and identifying compound mode of action via expression profiling. *Science*, **301**, 102–105.
8. Carrera,J., Rodrigo,G. and Jaramillo,A. (2009) Towards the automated engineering of a synthetic genome. *Mol. Biosyst.*, **5**, 733–743.
9. Gardner,T.S., Cantor,C.R. and Collins,J.J. (2000) Construction of a genetic toggle switch in *Escherichia coli*. *Nature*, **403**, 339–342.
10. Guido,N.J., Wang,X., Adalsteinsson,D., McMillen,D., Hasty,J., Cantor,C.R., Elston,T.C. and Collins,J.J. (2006) A bottom-up approach to gene regulation. *Nature*, **439**, 856–860.
11. Hasty,J., Isaacs,F., Dolnik,M., McMillen,D. and Collins,J.J. (2001) Designer gene networks: towards fundamental cellular control. *Chaos*, **11**, 207–220.
12. McMillen,D., Kopell,N., Hasty,J. and Collins,J.J. (2002) Synchronizing genetic relaxation oscillators by intercell signaling. *Proc. Natl Acad. Sci. USA*, **99**, 679–684.
13. Raser,J.M. and O'Shea,E.K. (2004) Control of stochasticity in eukaryotic gene expression. *Science*, **304**, 1811–1814.
14. Acar,M., Becskei,A. and van Oudenaarden,A. (2005) Enhancement of cellular memory by reducing stochastic transitions. *Nature*, **435**, 228–232.
15. Breeden,L.L. (2003) Periodic transcription: a cycle within a cycle. *Curr. Biol.*, **13**, R31–R38.
16. Chen,K.C., Calzone,L., Csikasz-Nagy,A., Cross,F.R., Novak,B. and Tyson,J.J. (2004) Integrative analysis of cell cycle control in budding yeast. *Mol. Biol. Cell*, **15**, 3841–3862.
17. Elowitz,M.B., Levine,A.J., Siggia,E.D. and Swain,P.S. (2002) Stochastic gene expression in a single cell. *Science*, **297**, 1183–1186.
18. Volfson,D., Marciniak,J., Blake,W.J., Ostroff,N., Tsimring,L.S. and Hasty,J. (2006) Origins of extrinsic variability in eukaryotic gene expression. *Nature*, **439**, 861–864.
19. Becskei,A. and Serrano,L. (2000) Engineering stability in gene networks by autoregulation. *Nature*, **405**, 590–593.
20. Bennett,M.R., Pang,W.L., Ostroff,N.A., Baumgartner,B.L., Nayak,S., Tsimring,L.S. and Hasty,J. (2008) Metabolic gene regulation in a dynamically changing environment. *Nature*, **454**, 1119–1122.
21. Basu,S., Gerchman,Y., Collins,C.H., Arnold,F.H. and Weiss,R. (2005) A synthetic multicellular system for programmed pattern formation. *Nature*, **434**, 1130–1134.
22. Simpson,M.L., Cox,C.D. and Sayler,G.S. (2003) Frequency domain analysis of noise in autoregulated gene circuits. *Proc. Natl Acad. Sci. USA*, **100**, 4551–4556.
23. Blake,W.J., Kærn,M., Cantor,C.R. and Collins,J.J. (2003) Noise in eukaryotic gene expression. *Nature*, **422**, 633–637.
24. Wang,X., Hao,N., Dohlman,H.G. and Elston,T.C. (2006) Bistability, stochasticity, and oscillations in the mitogen-activated protein kinase cascade. *Biophys. J.*, **90**, 1961–1978.
25. Blake,W.J., Balazsi,G., Kohanski,M.A., Isaacs,F.J., Murphy,K.F., Kuang,Y., Cantor,C.R., Walt,D.R. and Collins,J.J. (2006) Phenotypic consequences of promoter-mediated transcriptional noise. *Mol. Cell*, **24**, 853–865.
26. Smith,M., Sumner,E. and Avery,S. (2007) Glutathione and gts1p drive beneficial variability in the cadmium resistances of individual yeast cells. *Mol. Microbiol.*, **66**, 699.
27. Bayer,T., Hoff,K., Beisel,C., Lee,J. and Smolke,C. (2009) Synthetic control of a fitness tradeoff in yeast nitrogen metabolism. *J. Biolo. Eng.*, **3**, 1.
28. Nevozhay,D., Adams,R., Murphy,K., Josić,K. and Balázsi,G. (2009) Negative autoregulation linearizes the dose–response and suppresses the heterogeneity of gene expression. *Proc. Natl Acad. Sci. USA*, **106**, 5123.
29. Austin,D.W., Allen,M.S., McCollum,J.M., Dar,R.D., Wilgus,J.R., Sayler,G.S., Samatova,N.F., Cox,C.D. and Simpson,M.L. (2006) Gene network shaping of inherent noise spectra. *Nature*, **439**, 608–611.
30. Cookson,S., Ostroff,N., Pang,W.L., Volfson,D. and Hasty,J. (2005) Monitoring dynamics of single-cell gene expression over multiple cell cycles. *Mol. Syst. Biol.*, **1**, msb4100032.
31. Egilmez,N.K. and Jazwinski,S.M. (1989) Evidence for the involvement of a cytoplasmic factor in the aging of the yeast *Saccharomyces cerevisiae*. *J. Bacteriol.*, **171**, 37–42.
32. Slater,M., Sharrow,S. and Gart,J. (1977) Cell cycle of Saccharomyces cerevisiae in populations growing at different rates. *Proc. Natl Acad. Sci. USA*, **74**, 3850–3854.
33. Egilmez,N., Chen,J. and Jazwinski,S. (1990) Preparation and partial characterization of old yeast cells. *J. Gerontol.*, **45**, B9.

Cell cycle dependent variations in protein concentration (Supplementary Data)

Natalie A. Cookson[1], Scott W. Cookson[1], Lev S. Tsimring[2] & Jeff Hasty[1,2,3]

1. Department of Bioengineering, University of California, San Diego, La Jolla, CA 92093
2. BioCircuits Institute, University of California, San Diego, La Jolla, CA 92093
3. Molecular Biology Section, Division of Biology, University of California, San Diego, La Jolla, CA 92093

Forward scatter size calibration

In order to compare our microscopy size data to the FSC histogram provided by the flow cytometer, we had to first determine what size dimension the FSC data represents. To do this, we used spherical flow calibration beads of various diameters ranging from 2 to 15 μm (SPHERO^{TM} Flow Cytometry Size Standard Kit, http://www.spherotech.com/FlowCytometrySizeStd.htm). Using a Becton-Dickinson FACSCalibur flow cytometer, we ran these beads through on the same settings we use to collect our yeast data. For each size bead, we collected 50,000 samples, and we used MATLAB (The MathWorks, Inc.) to calculate the mean FSC measurement. In order to determine if the FSC was proportional to the length, area, or volume of a sphere, we compared the diameter, diameter^2, and diameter^3 of the beads to the mean FSC value. It is clear from our data that the FSC measurement is proportional to the diameter of the bead (Figure S1). Also, a linear fit to the diameter vs. FSC data provides a nice equation to convert FSC to length.

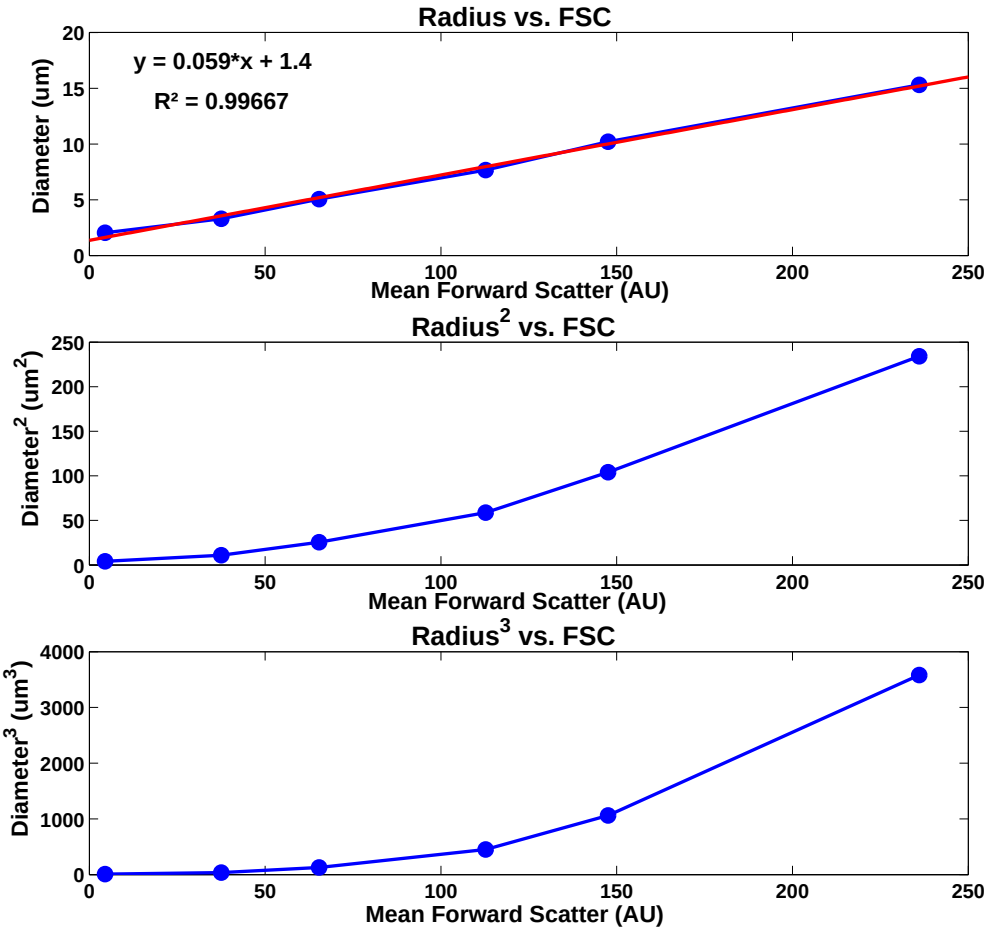

Figure S1: Size data for flow calibration beads. The top panel compares the diameter of the beads to the mean forward scatter reported by the flow cytometer. The bottom panel compares the diameter squared (area) of the beads, and the bottom compares the diameter cubed (volume) of the beads to the forward scatter.

Fluorescence Integration

In order to measure total fluorescence emitted by a single cell, we must be able to assume that our image acquisition method is able to capture the fluorescence signal from the entire cell. Wide-field microscopy is ideal for this purpose, as a wide-field microscope collects the light from all points in the focal plane at once plus all the light from illuminated regions of the sample that are above and below the focal plane. In addition, a 40x objective was chosen in order to strike a good balance between fluorescence signal, depth of field, and field of view.

The depth of field (the axial range through which an objective can be focused without any appreciable change in image sharpness) of the 40x oil objective used is about 1.0 μm. While light outside of this region will be collected, this signal may not be integrated linearly. However, as the imaging region is only 4 μm high, and the cells are confined to a monolayer within this region, the loss of light due to out-of-focus regions of a cell's volume is likely insignificant and should effect all cells in a similar manner. As a check to ensure that images were composed of light emitted from all regions of the cell, we examined the fluorescence profile extracted along the major axis of a healthy adult cell. Assuming an ellipsoidal cell shape and nonspecific YFP localization, we would expect this fluorescence profile to fit an elliptical curve created based on the major and minor axis dimensions of the cell.

Below, this verification is demonstrated, with a high degree of correlation (Figure S2). Slight imperfections in the correlation may be due to deviations from a purely ellipsoidal cell shape as well as the imperfect distribution of YFP throughout the cellular volume. Fluorescent proteins should not be localized to any particular area and should be robust to pH differences, so we expect the signal to be more or less constant throughout the cellular volume. However, since we are measuring the fluorescence of the cell as a whole, the accurate measurement of total fluorescence does not rely on the homogeneity of the fluorescent protein.

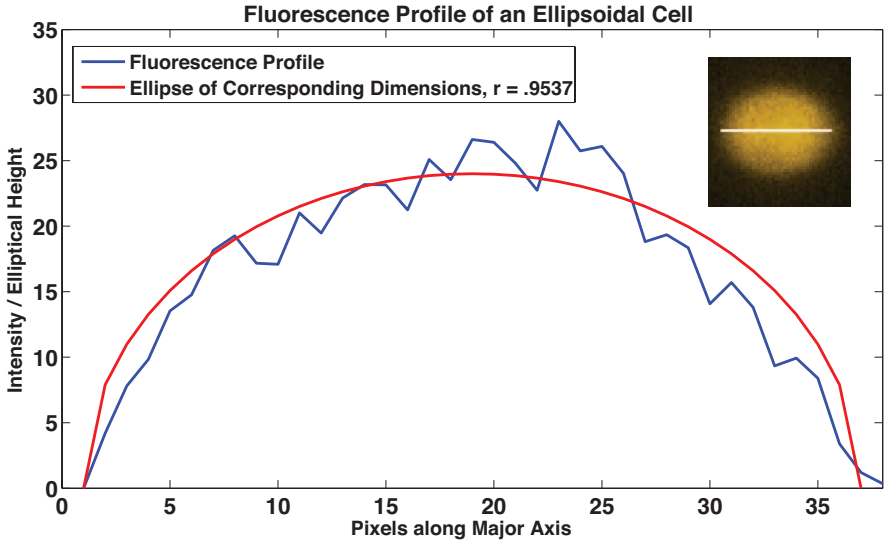

Figure S2: Correlation between the fluorescence profile of a cell taken along its major axis (inset) and the corresponding elliptical shape.

Volume Growth Characteristics

We have made our MATLAB code available at:

biodynamics.ucsd.edu/YeastVolume/YeastGrowth.m

This code details the values used for each of the characteristics that we measured and integrated into the cell volume model. All size measurements were normalized so that the average adult cell had a mean maximum volume (volume attained at the end of each cell cycle) of 1.0. The characteristics measured were the following:

- Initial Size: The volume of a newly budded daughter cell.
- Maximum Size: The maximum volume reached by a cell at the end of each cell division cycle.
- Cycle Growth: The volume increase over a single cell division cycle.
- Cycle Time: Time to complete the cell division cycle.
- Epsilon: Fraction of volume the mother retains at bud event.
- G1 Fraction: Fraction of cell cycle time spent in G1 phase.
- G1 Rate: Growth rate for G1 phase.
- S Rate: Growth rate for S phase.
- Fluor. Rate: Rate of YFP production.
- Initial Fluor.: Initial YFP level in a new cell.
- Initial Conc.: Inital YFP concentration in a new cell.

In the table below, we detail the mean and standard deviation of each of these characteristics. If a characteristic changed throughout the early generations (gen #), we document the specific value for each cycle, until the value leveled off (at which point we leave the table blank).

We also measured the growth rate in batch culture of this strain, using the standard OD_{600} technique and found a doubling time of 86.6 minutes, which corresponds with the mean cycle time for a healthy adult cell (Figure S3).

Characteristic	Gen 1	Gen 2	Gen 3	Gen 4	Gen 5	Gen 6	Gen 7
Initial Size Mean	0.4532						
Initial Size Std.	0.0772						
Max. Size Mean	1.0						
Max. Size Std.	0.1199						
Cycle Growth Mean	0.3577						
Cycle Growth Std.	0.0948						
Cycle Time Mean	143.20	104.42	86.64				
Cycle Time Std.	31.00	26.32	11.50				
Epsilon Mean	0.5963	0.6367	0.6443	0.6650	0.6656	0.6703	0.6760
Epsilon Std.	0.0479	0.0522	0.0483	0.0489	0.0470	0.0474	0.0513
G1 Fraction Mean	0.611	0.523	0.511				
G1 Fraction Std.	0.097	0.112	0.094				
G1 Rate Mean	0.0014						
G1 Rate Std.	0.000099						
S Rate Mean	0.0082						
S Rate Std.	0.003						
Fluor. Rate Mean	2,426	3,163	3,789	4,061	4,313		
Fluor. Rate Std.	1,039	882	908	1,083	1,004		
Initial Fluor. Mean	267,800						
Initial Fluor. Std.	100,500						
Initial Conc. Mean	583,530						
Initial Conc. Std.	156,860						

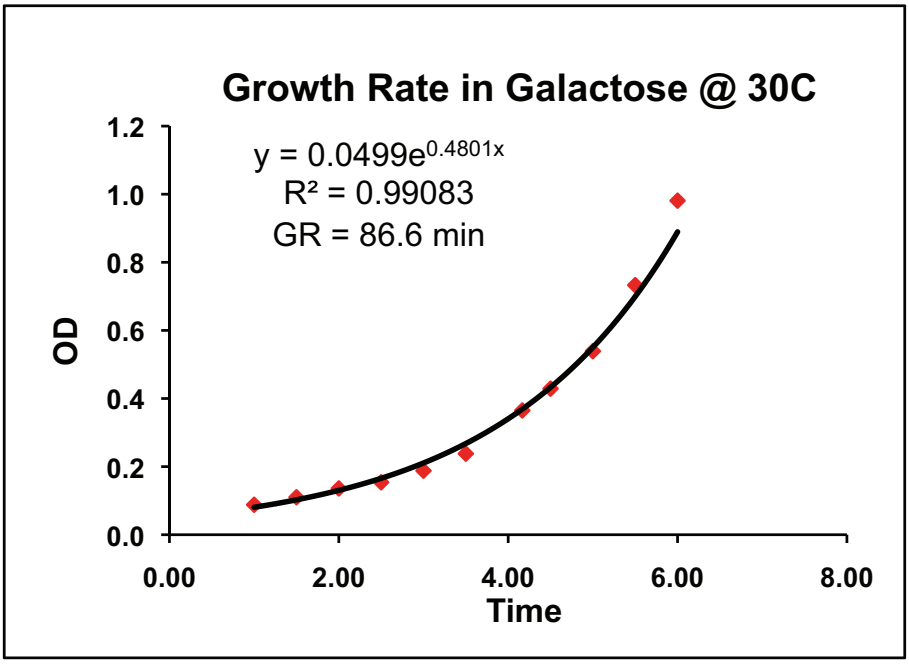

Figure S3: Growth rate calculated by measuring the OD_{600} over time.